Measuring the second-order coherence of a nanolaser by intracavity frequency doubling

Yasutomo Ota,[1,*] Katsuyuki Watanabe,[1] Satoshi Iwamoto,[1,2] and Yasuhiko Arakawa[1,2]

[1]*Institute for Nano Quantum Information Electronics, The University of Tokyo, 4-6-1 Komaba, Meguro-ku, Tokyo 153-8505, Japan*

[2]*Institute of Industrial Science, The University of Tokyo, 4-6-1 Komaba, Meguro-ku, Tokyo 153-8505, Japan*

(Received 12 December 2013; published 18 February 2014)

We measured the second-order coherence at zero time delay, $g^{(2)}(0)$, of a high-Q photonic crystal nanocavity quantum dot laser below and above the lasing threshold, via detecting visible emission originated from the second harmonic generation (SHG) occurring within the laser cavity. The efficiency of the nonlinear frequency conversion process, defined by SHG intensity divided by the square of laser output intensity, is shown to be proportional to $g^{(2)}(0)$, and hence is used for the measurement. The obtained $g^{(2)}(0)$ values show good agreement with those measured by a Hanbury Brown–Twiss interferometer equipped with ultrafast superconducting single-photon detectors.

DOI: 10.1103/PhysRevA.89.023824 PACS number(s): 42.55.Sa, 42.50.Ar, 42.65.Ky

I. INTRODUCTION

Recently, various types of novel nanolasers, including semiconductor micro- and nanocavity lasers [1–6], metal-coated nanocavity lasers [7,8], and plasmonic nanolasers [9,10], have emerged and formed a new frontier of laser science. One characteristic of such nanolasers, distinguishing them from conventional bulky lasers, is a high spontaneous emission coupling factor, β, which is defined as the fraction of spontaneous emission that directly couples to the laser cavity mode. A large value of β is advantageous for lowering the lasing threshold [11,12] and increasing the direct intensity modulation speed [3,11]. In contrast, large β is sometimes detrimental, in that it tends to increase the relative intensity noise [13,14] and decrease the coherence time [15] of the laser output. This fact has motivated various theoretical [13,16,17] and experimental [4,14,18–21] studies aiming at understanding intensity noise properties of high-β lasers.

One way to characterize the intensity noise properties is by measuring the second-order coherence, $g^{(2)}(t)$, and particularly its zero time delay value, $g^{(2)}(0)$ $(=\langle I^2\rangle/\langle I\rangle^2$, where I is the laser output intensity). A frequently used technique is Hanbury Brown and Twiss (HBT) interferometry, which typically uses a pair of photon detectors together with an electronic coincidence counter, and can directly measure $g^{(2)}(t)$. Generally, this method has a fairly limited timing resolution mainly due to slow photon detectors, and tends to lose accuracy when measuring the $g^{(2)}(t)$ curves of nanolasers [4,18] operating below the lasing threshold, which are likely to show rapid decays roughly at the cavity decay rates ($\propto 1/Q$). Recently, the detector timing resolution has been improved largely in some photon counters [for example, superconducting single-photon detectors (SSPDs)], but is still on the order of tens of picoseconds in most cases [14,21,22]. Photon counting streak cameras [19,23–25] are an alternative choice of detector that can access subpicosecond timing resolutions. However, the camera usually has a low detection efficiency and seems not to be suitable for measuring weak outputs from high-Q and high-β nanolasers operating near the threshold. In addition to these methods, techniques based on interpolation from $g^{(1)}(t)$ measurements [20] and on pulsed homodyne detection [26,27] are used for measuring $g^{(2)}(0)$, but none of these have been applied for high-β nanolasers operating near and below threshold.

At another frontier of research, two-photon processes, such as two-photon absorption [28] and second harmonic generation (SHG) [29–31], have been investigated as measurement tools for the intensity noise properties of light. In general, these two-photon processes have efficiencies proportional to $g^{(2)}(0)$ and occur within the femtosecond time scale dictated by the uncertainty principle. Thus, they have been successfully utilized for ultrafast $g^{(2)}(0)$ measurements. However, such high order optical processes are inherently weak and require strong light intensity, resulting in the limited use for only measuring the strong output from bulky lasers, so far.

One possible way to improve the multiphoton process efficiency is via photonic micro- and nanostructures with strong optical confinement capabilities, such as whispering gallery mode resonators [32–34], photonic nanowires [35,36], plasmonic structures [37,38], and photonic crystals (PhCs) [39–45]. Recently, we have demonstrated efficient intracavity SHG [46] and sum frequency generation [47] using photonic crystal nanocavity lasers that exhibit simultaneously high Qs and small mode volumes (Vs). This efficient intracavity SHG process may be useful for measuring $g^{(2)}(0)$ of such high-β nanolasers.

In this work, we report a measurement of the second-order coherence of a high-β nanolaser by intracavity SHG efficiently occurring within the laser cavity. We investigated a quantum dot (QD) nanolaser with a GaAs-based PhC nanocavity that exhibits a high Q and small V, and measured its $g^{(2)}(0)$ values even far below the lasing threshold. First, we present a quantum theory of intracavity SHG and clarify the condition that the efficiency of SHG, η, which is defined by SHG power over the square of laser output power, is proportional to $g^{(2)}(0)$. This condition matches well with our experimental condition. Second, we discuss the results of SHG efficiencies measured by μ photoluminescence (PL) and compare them with $g^{(2)}(0)$ values obtained by a HBT setup using a pair of ultrafast SSPDs. The two values show fairly good agreement, demonstrating the validity of the $g^{(2)}(0)$ measurement by using the intracavity SHG. The presented method is simple and does not require special detectors but enables an ultrafast

*ota@iis.u-tokyo.ac.jp

measurement of $g^{(2)}(0)$, which could be applicable to various types of high-β nanolasers, since many of them are made from III-V semiconductors, which in general possess large second-order nonlinear susceptibilities, and have high Q/V values that enable the efficient intracavity SHG [η in general scales as $(Q/V)^2$].

II. THEORY

It is well known that a two-photon process using a single mode of light occurs with a probability proportional to $g^{(2)}(0)$ [28,29,48]; however, it is nontrivial whether this is the case also for nonlinear optical processes invoked within nanoscale photonic media. In this section, we theoretically discuss the efficiency of intracavity SHG, η, and its relation to $g^{(2)}(0)$ using a quantum master equation model. We consider a cavity mode at frequency ω_b in the near infrared (NIR) that couples to multiple visible (VIS) modes through the second-order nonlinear optical interaction. The NIR mode is considered to be exposed to phenomenological coherent and incoherent optical pumping, in order to represent the intracavity optical field below (thermal-like) and above (coherentlike) the lasing threshold. This model can be regarded as an extension of previous studies [49–52] and differs from our previous report [46] by the addition of the incoherent pumping. The Hamiltonian of the system, H, under an appropriate rotating frame is expressed as

$$\frac{H}{\hbar} = \sum_k \Delta_k a_k^\dagger a_k + (Eb^\dagger + E^* b) + \sum_k g_k (a_k^\dagger b^2 + a_k b^{\dagger 2}). \tag{1}$$

$\Delta_k = \omega_a^k - 2\omega_b$ is the detuning between the kth VIS mode at a frequency of ω_a^k and the generated second harmonic light at $2\omega_b$. a_k and b are the annihilation operators for the kth VIS mode and the NIR mode, respectively. E is the strength of the coherent drive for the NIR mode. g_k is the nonlinear optical coupling strength between the NIR and the kth VIS mode:

$$g_k = \epsilon_0 \left(\frac{\hbar}{2\epsilon_0}\right)^{3/2} \sqrt{\frac{\omega_b^2 \omega_a^k}{\epsilon_b^2 \epsilon_a V_b^2 V_a^k}} \int \chi^{(2)}_{lmn}(r) b_l(r) b_m(r) a_n^k(r) dV. \tag{2}$$

In the equation for g_k, ϵ_0 is the vacuum permittivity and ϵ_a (ϵ_b) is the relative permittivity of the host optical medium at the VIS (NIR) mode frequency. V_a^k and V_b are the mode volumes of the kth VIS and NIR optical modes, respectively. $\chi^{(2)}_{lmn}(r)$ is the second order nonlinear susceptibility tensor of the host material, where r represents the position within the volume integral. $b(r)$ and $a^k(r)$ are the normalized spatial field distributions of the NIR and kth VIS modes, respectively. The repeated index summation convention is used within the integral (regarding l,m,n) and the integration is performed over all space. For achieving a large g_k, it is important to employ a large $\chi^{(2)}_{lmn}$, small V_a^k and V_b, appropriate choice of the nonlinear crystal axis orientation [45], and large constructive spatial overlap between the related modes. In our situation, the conventional requirement of phase matching is replaced by the demand of the large spatial overlap. A system density operator ρ evolves in time by the following master equation:

$$\frac{d\rho}{dt} = -\frac{i}{\hbar}[H,\rho] + L\rho. \tag{3}$$

$L\rho$ corresponds to the system reservoir interaction term, which contains three contributions:

$$\begin{aligned} L\rho = {} & \frac{P}{2}(2b^\dagger \rho b - bb^\dagger \rho - \rho bb^\dagger) \\ & + \frac{\kappa + P}{2}(2b\rho b^\dagger - b^\dagger b\rho - \rho b^\dagger b) \\ & + \sum_k \frac{\kappa_a^k}{2}(2a_k \rho a_k^\dagger - a_k^\dagger a_k \rho - \rho a_k^\dagger a_k). \end{aligned} \tag{4}$$

The first two terms, respectively, express an incoherent pump to the NIR mode at a rate of P and a cavity photon leakage at κ. The second term also includes an influence from the pump [53]. The third term is the sum of photon leakage from each VIS mode (the kth mode leaks at a rate of κ_a^k). Using the equations above, one easily obtains a set of evolution equations for the expectation values:

$$\frac{d\langle a_k^\dagger a_k\rangle}{dt} = i g_k \langle a_k b^{\dagger 2} - a_k^\dagger b^2\rangle - \kappa_a^k \langle a_k^\dagger a_k\rangle, \tag{5}$$

$$\begin{aligned} \frac{d\langle a_k^\dagger b^2\rangle}{dt} = {} & i g_k \langle a_k^\dagger a_k(-2 - 4b^\dagger b) + b^{\dagger 2} b^2\rangle \\ & + i \sum_{l\neq k} g_k \langle a_l a_k^\dagger b^{\dagger 2} b^2 - a_l^\dagger a_k b^2 b^{\dagger 2}\rangle \\ & - i2E\langle a_k^\dagger b\rangle + \left(i\Delta_k - \frac{\kappa_a^k}{2} - \kappa\right)\langle a_k^\dagger b^2\rangle. \end{aligned} \tag{6}$$

In the steady state ($\frac{d}{dt} = 0$), these equations can be summarized after neglecting the term related to simultaneous excitation of multiple VIS modes:

$$\begin{aligned} & \frac{\left(\frac{\kappa_a^k}{2} + \kappa\right)^2 + \Delta_k^2}{2\left(\frac{\kappa_a^k}{2} + \kappa\right)} \kappa_a^k \langle a_k^\dagger a_k\rangle \\ & = g_k^2 \langle a_k^\dagger a_k(-2 - 4b^\dagger b) + b^{\dagger 2} b^2\rangle - g_k(E^*\langle a_k b^\dagger\rangle + E\langle a_k^\dagger b\rangle) \\ & \quad + \frac{i g_k \Delta_k}{\left(\frac{\kappa_a^k}{2} + \kappa\right)}(E^*\langle a_k b^\dagger\rangle - E\langle a_k^\dagger b\rangle). \end{aligned} \tag{7}$$

Assuming weak frequency conversion ($\langle a_k^\dagger a_k\rangle \ll \langle b^\dagger b\rangle$), fast photon leakage from the VIS modes, and a small nonlinear interaction strength ($\kappa_a^k \gg \kappa \gg g_k$), only the term $g_k^2\langle b^{\dagger 2} b^2\rangle$ in the right-hand side has a comparable quantity compared to the left-hand side, and remaining terms are smaller by at least a factor of $2\kappa/\kappa_a^k \ll 1$. These assumptions are usually fulfilled when many of the related experiments are performed. Then, Eq. (7) is reduced to

$$\frac{\left(\frac{\kappa_a^k}{2} + \kappa\right)^2 + \Delta_k^2}{2\left(\frac{\kappa_a^k}{2} + \kappa\right)} \kappa_a^k \langle a_k^\dagger a_k\rangle \approx g_k^2 \langle b^{\dagger 2} b^2\rangle = g_k^2 \langle b^\dagger b\rangle^2 g^{(2)}(0). \tag{8}$$

Finally, we obtain an expression for the nonlinear frequency conversion efficiency, η, which is defined as total SHG power ($\sum_k \hbar 2\omega_b \kappa_a^k \langle a_k^\dagger a_k\rangle$) divided by the square of the NIR laser

output power ($\hbar\omega_b\kappa\langle b^\dagger b\rangle$):

$$\eta = \frac{\sum_k \hbar 2\omega_b \kappa_a^k \langle a_k^\dagger a_k\rangle}{(\hbar\omega_b\kappa\langle b^\dagger b\rangle)^2} \tag{9}$$

$$\approx \frac{2}{\hbar\omega_b}\left[\sum_k \frac{4g_k^2}{\kappa_a^k\kappa^2}\frac{\left(\frac{\kappa_a^k}{2}\right)^2}{\left(\frac{\kappa_a^k}{2}\right)^2+\Delta_k^2}\right] g^{(2)}(0). \tag{10}$$

Equation (10) clearly demonstrates the linear relationship between η and $g^{(2)}(0)$. The prefactor $(g/\kappa)^2$ indicates a quadratic increase of η as Q/V increases [43,46].

In order to confirm the validity of Eq. (10), we performed numerical simulations by directly solving Eq. (3). We consider a case that there is a NIR mode at 1 eV and a single VIS mode that resonantly couples to the SHG light ($\Delta = 0$) with a g of 0.1 μeV. The NIR and VIS modes have Q factors of 10 000 and 100, respectively. This setting for the system parameters is chosen by reference to our previous report [46]. When the nonlinear frequency conversion is weak, we can set $E = \sqrt{r}\frac{\kappa}{2}\sqrt{N_{\rm ave}}$ and $P = (1-r)\kappa N_{\rm ave}$, where $N_{\rm ave}$ is the average photon number in the NIR mode. r determines the ratio of the coherent pump contribution to the incoherent pump. In the following calculation, we set $N_{\rm ave} = 1$. For several r values, we first simulate the average photon numbers for VIS ($\langle a^\dagger a\rangle$) and NIR ($\langle b^\dagger b\rangle$) and directly obtain η by using its original definition as in Eq. (9). Then, we simulate $g^{(2)}(0)$ for each r in order to calculate η using the approximation [Eq. (10)]. By changing r from 0 (P only) to 1 (E only), we can shift the photon statistics for the NIR mode from thermal to coherent, and hence gradually tune $g^{(2)}(0)$ from 2 to 1. A summary of the calculated η plotted as a function of $g^{(2)}(0)$ is shown in Fig. 1. The conversion efficiencies obtained from the original definition exhibit good agreement with those obtained using the approximation. The observed proportionality of η with respect to $g^{(2)}(0)$ suggests the possible usage of η as a measure of $g^{(2)}(0)$. The small deviation between the two η plots around $g^{(2)}(0) \sim 2$ probably arises from the truncation of the photon number space when solving Eq. (3). We also confirmed the validity of Eq. (10) for several other cases that include finite Δ's and/or multiple VIS modes.

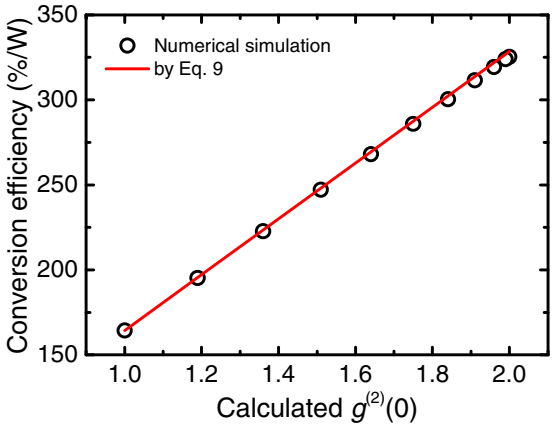

FIG. 1. (Color online) Simulated nonlinear frequency conversion efficiency, η, as a function of calculated $g^{(2)}(0)$. Black circles: Results directly calculated by the original definition of η [Eq. (9)]. Red line: Results obtained by using the approximation [Eq. (10)].

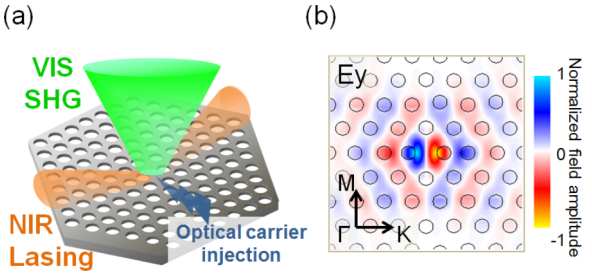

FIG. 2. (Color online) (a) Schematic illustration of the investigated PhC nanolaser. The nanolaser emits coherent NIR light under optical carrier injection and simultaneously VIS light via intracavity SHG using the internally generated NIR light. (b) Electric field distribution of the fundamental mode of the H0 nanocavity, which supports the NIR lasing in this study.

When the related optical modes are influenced by additional absorption losses, the photon loss rates for the kth VIS and NIR modes increase and should be rewritten to $\kappa_a^k + \kappa_{a,\rm abs}^k$ and $\kappa + \kappa_{\rm abs}$, respectively. Even in this case, the expression for η is modified marginally, under an assumption of $\kappa_a^k + \kappa_{a,\rm abs}^k \gg \kappa + \kappa_{\rm abs}$:

$$\eta \approx \frac{2}{\hbar\omega_b}\left[\sum_k \frac{4g_k^2}{\kappa_a^k\kappa^2}\frac{\left(\frac{\kappa_a^k}{2}\right)^2}{\left(\frac{\kappa_a^k+\kappa_{a,\rm abs}^k}{2}\right)^2+\Delta_k^2}\right] g^{(2)}(0). \tag{11}$$

Since g_k, κ, κ_a^k, and Δ_k are predominantly determined by the photonic structure under consideration, they can be regarded as constant during experiments for individual nanolasers. Thus, as long as the absorption for the VIS modes ($\kappa_{a,\rm abs}^k$) is constant or its change negligibly affects η, we can use η as a measure of $g^{(2)}(0)$. This is the case in which we performed experiments as presented below.

III. EXPERIMENT

A. Sample structure and experimental setup

A schematic of the investigated nanolaser is shown in Fig. 2(a). We investigated a GaAs-based H0 photonic crystal nanocavity [6,54] containing InAs quantum dots as gain media. The nanolaser lases in the NIR (~1100 nm) under optical carrier injection and simultaneously emits green light (~550 nm) via intracavity SHG. The air-bridge PhC slab has a thickness d of 180 nm, and contains five layers of InAs QDs (with an areal density of $\sim 3.6 \times 10^{10}$ cm^2 per layer). The QD ground state PL is centered around 1100 nm at 10 K. The two-dimensional triangular PhC lattice was designed with a lattice constant $a = 340$ nm and air hole radius $r = 99$ nm. A top view of the cavity, overlaid with the fundamental mode field distribution, is shown in Fig. 2(b). Two air holes around the cavity center are shifted by $0.14a$ outward along the Γ-K direction and the third nearest air holes along with this direction are also shifted by $0.06a$. The first and second nearest holes along the Γ-M direction from the cavity center are, respectively, shifted outward by $0.04a$ and $0.02a$. This design results in a cavity Q factor of 93 000 and a V of $0.25(\lambda/n)^3$ for the fundamental mode, calculated by finite difference time domain simulations [54]. The cavity was patterned by standard PhC fabrication processes on a slab grown on a

(001)-oriented GaAs wafer, such that the Γ-K axis of the PhC lattice directs along with the [110] orientation of the GaAs. It is noteworthy that the nonlinear frequency conversion efficiency drops roughly one order of magnitude when we tilt the cavity by 45° around the growth axis. Optical characterization was performed by using a confocal μ-PL setup at 30 K. The excitation source was a continuous wave laser diode oscillating at 808 nm and was focused onto the sample surface by an objective lens with a numerical aperture of 0.6. The excitation power is defined as that measured after the objective lens. PL collected by the same objective lens was split into the NIR and VIS signals by a dichroic beam splitter and separately sent to spectrometers equipped with liquid nitrogen cooled multichannel detectors. The spectral resolution for the NIR (VIS) was $\sim$40 μeV ($\sim$1.2 meV). The intensities of the NIR (VIS) emissions were evaluated by convolutional (simple peak) fitting of the obtained spectra. A HBT interferometer was built by a combination of a spectrometer as a bandpass filter (filter bandwith = 640 μeV), a 50:50 beam splitter, and two superconducting single-photon detectors equipped at the end of optical fibers in a liquid-helium container. Overall, the timing resolution of our setup is $\sim$56 ps.

B. Emission characteristics both at the NIR and VIS

First, we investigated the output characteristics of the nanolaser both in the NIR and VIS. Figures 3(a)–3(c), respectively, show a light-in versus light-out (LL) plot for the NIR output, a spectrum taken above the lasing threshold, and the behavior of the cavity linewidth as a function of the pumping power. The LL plot shows a nonlinear increase of the output power accompanied by lasing oscillation with a threshold at 8.2 μW, determined at the inflection point. The lasing spectrum taken at a pump power of 42 μW exhibits single-mode lasing at a wavelength of 1106 nm. A linewidth narrowing is clearly observed, and a cold cavity Q factor of 17 000 (linewidth of 66 μeV) is estimated at the lower power edge of the transition region (corresponding pumping power: 3 μW). We analyze the LL curve through fitting to a laser rate equation model [12,25,55]:

$$\frac{dn}{dt} = -\kappa n + \beta\gamma Nn + \beta\gamma N, \quad \frac{dN}{dt} = P - \gamma N - \beta\gamma Nn. \tag{12}$$

Here, n and N are intracavity photon number and population inversion, respectively, and κ, γ, and β respectively correspond to the cavity decay rate, spontaneous emission rate, and spontaneous emission coupling factor. We assume κ = 100 GHz (66 μeV) from the measured cold cavity Q factor. γ is set to be 8 GHz, from fitting to data as discussed in Appendix B. This value is several times faster than those measured for as-grown QDs, presumably due to the Purcell effect in the high Q/V nanocavity. The best fit to the experimental curve was obtained for $\beta = 0.12$ and the calculated LL curve is overlaid in Fig. 3(a). From the fit, the average intracavity photon number at each pumping power can be deduced [see the right axis of Fig. 3(a)]. We also investigated SHG from the same nanolaser in the VIS wavelength region, and plot its LL curve and an emission spectrum, respectively, in Figs. 3(d) and 3(e). The LL curve for the SHG shows a highly nonlinear increase and the emission spectrum exhibits a sharp emission line at a wavelength of 553 nm (half the wavelength of the NIR lasing mode). The SHG signal is observable even under weak

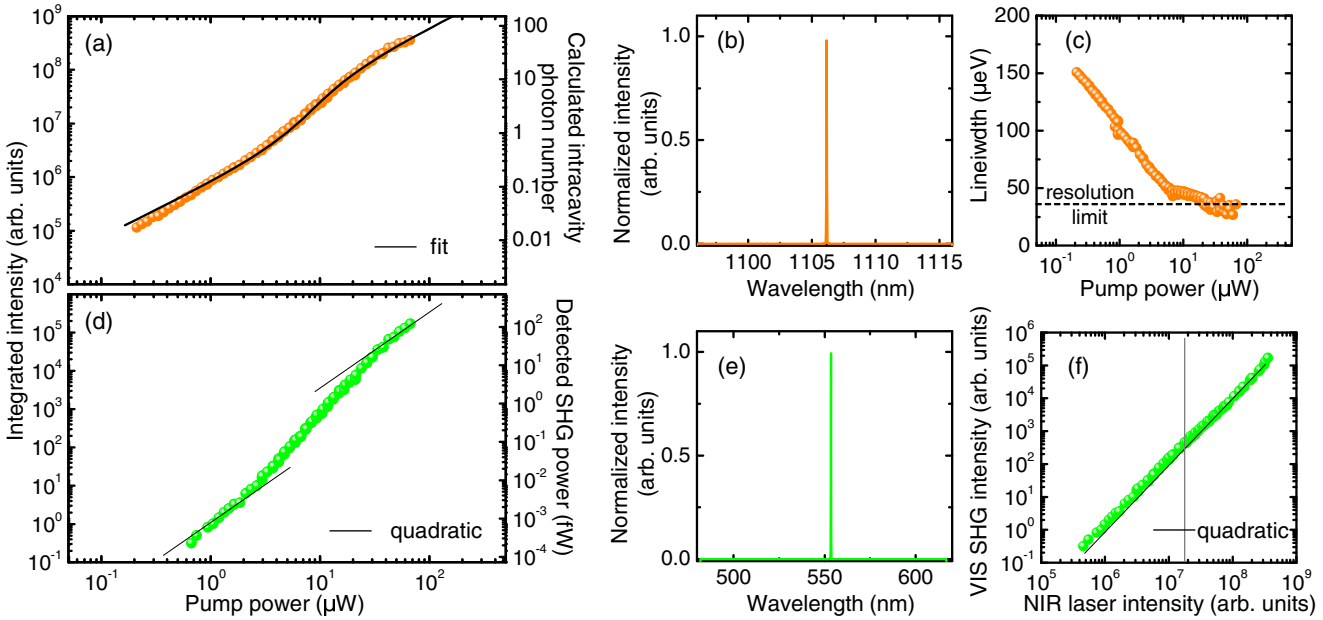

FIG. 3. (Color online) (a) LL plot for the NIR lasing mode output. Solid line is a fit by a laser model using Eq. (12). (b) NIR lasing spectrum taken under a pump power of 42 μW. (c) Linewidths plotted as a function of the pumping power. The resolution of our spectrometer (34 μeV) is shown as a horizontal dashed line. (d) LL plot for the VIS mode output. Two solid lines are a guide for the eye showing quadratic increase of the LL curve. (e) VIS emission spectrum taken under a pump power of 42 μW. (f) VIS emission intensity plotted as a function of the NIR output intensity. Diagonal solid line is a guide for the eye indicating the quadratic increase. Dashed vertical line indicates the NIR intensity at the lasing threshold.

pumping power conditions down to 0.67 μW, which is much below the NIR lasing threshold. At this pump power, only 0.07 photons are estimated to exist in the NIR mode on average. The maximum detected SHG power (estimated from the detector count) was 122 fW at a pump power of 67 μW. The NIR laser output at the same pump power was 970 nW. Therefore, the nonlinear frequency conversion efficiency η was estimated to be 13%/W. We note that this value is a lower limit, since we compared the ideally estimated NIR output power with experimentally measured SHG power, which is imperfectly collected by objective lens and significantly attenuated by numerous optics before the detection. In Fig. 3(f), the VIS emission power is plotted as a function of the measured NIR intensity. Overall, the VIS output quadratically increases with respect to the NIR output. However, a deviation from the quadratic increase can be seen around the NIR output at the lasing threshold (gray vertical line). We consider that this deviation arises from the change of the photon statistics [or $g^{(2)}(0)$] of the NIR laser field. This point will be discussed in detail later. It is also worth noting that the emission linewidth for the SHG is observed to be twice larger than that for the fundamental NIR lasing mode, as discussed in Appendix A.

C. HBT measurement

Next, we performed $g^{(2)}(t)$ measurements on the same nanolaser by using the HBT setup, which was able to measure $g^{(2)}(t)$ even below the lasing threshold, thanks both to an ultrafast response of the detector ($\sim$56 ps as a total system) and the high Q (i.e., slow photon escape) of the nanolaser. Figure 4 shows several $g^{(2)}(t)$ curves obtained at different pumping powers. Sufficiently below the lasing threshold, a monotonic decay of the curve from the time origin was observed (see the 0.62 μW pumping case), as a result of the generation of the thermal-like state in the cavity. A flat $g^{(2)}(t)$ curve is observed much above the lasing threshold (see the 39 μW pumping case), indicating that coherentlike state of light is generated in the nanolaser. Through fits to the two curves (for details, see Appendix B), we obtained $g^{(2)}(0)$ values of 1.4 and 1.0 for the 0.62 and 39 μW pump cases, respectively. Details of the transition of $g^{(2)}(0)$ around the lasing threshold will be discussed using Fig. 5 later. Interestingly, around the lasing threshold, we detected oscillatory behavior in the $g^{(2)}(t)$ curves. These seem to be in line with recent reports of experimentally observed oscillating $g^{(2)}(t)$ curves in several types of microscale semiconductor lasers [19,25] by ultrafast photon counting streak cameras: Moreover, the existence of the oscillation is theoretically predicted also for high-β nanolasers under continuous wave operation [17] (see Appendix B).

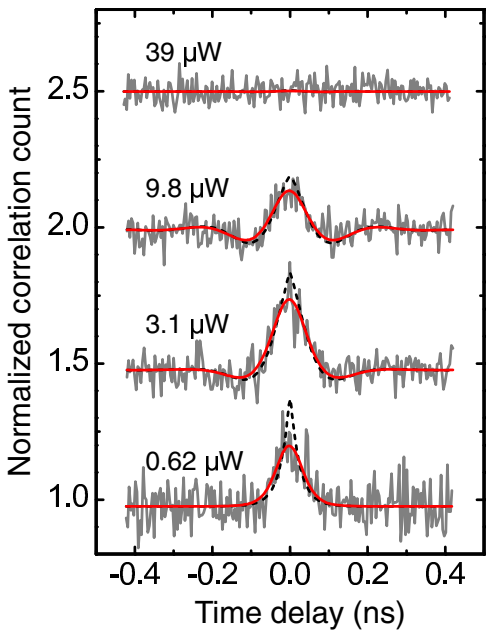

FIG. 4. (Color online) $g^{(2)}(t)$ curves measured by the HBT setup under various pumping powers. Gray lines, smooth red solid lines, and black dashed lines, respectively, are experimental data, fit results, and deconvolved fit curves. Plots for 3.1, 9.8, and 39 μW have offsets of 0.5, 1, and 1.5, respectively.

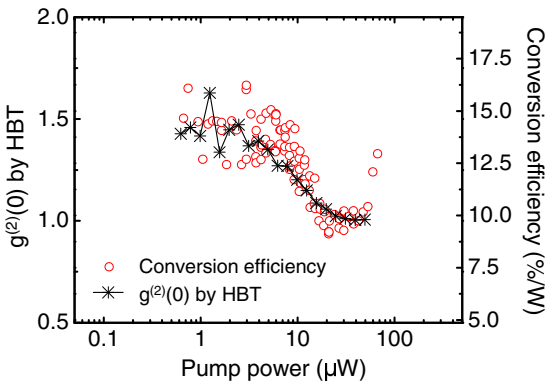

FIG. 5. (Color online) Comparison between $g^{(2)}(0)$ measured by the HBT setup and η by μPL. $\eta = 9.7\%$/W is plotted at the same level of $g^{(2)}(0) = 1$. The vertical axis for η has been linearly scaled as the $g^{(2)}(0)$ axis $\times$ 9.7, enabling direct comparison between the two data sets.

D. Comparing η with $g^{(2)}(0)$ values obtained by HBT

Finally, we compare the values of $g^{(2)}(0)$ obtained from $g^{(2)}(t)$ curves measured in the HBT experiments, and those estimated from the SHG efficiencies, η's. Both sets of data are plotted in Fig. 5. First, we focus on the values η (red circle). Below the lasing threshold (for pump powers from 0.7 to 3 μW), η remains at 15%/W. The values smoothly decrease around the pump powers corresponding to the laser transition region (3–20 μW). η's, then flattens at $\sim$ 10%/W for pump powers more than 20 μW, in which the LL curve for the NIR mode is in the linear region. Around the highest pumping power, a sudden jump of η is seen: We do not have any suitable explanation for this unexpected behavior at this stage. The origin of scatter in the data may be attributed to the instability of the μ-PL setup that induces fluctuation in the measured emission intensities. Next, we discuss the transition of $g^{(2)}(0)$ values taken by the HBT measurements (the values come from the deconvolved fit curves). The $g^{(2)}(0)$ values below and above the lasing threshold smoothly change from $\sim$1.4 to 1. This smooth transition, and $g^{(2)}(0)$ values much lower than 2 when below the lasing threshold, are characteristics of high-β lasers.

Now, we compare the two results. We note that, in Fig. 5, $\eta = 9.7\%/\mathrm{W}$ is plotted at the same level of $g^{(2)}(0) = 1$, and the vertical axis for η is scaled such that it is directly proportional to the $g^{(2)}(0)$ axis [$g^{(2)}(0)$ value multiplied by 9.7], enabling a direct comparison of the linear relationship between the two sets of data. A fairly good agreement between the two measurements proves that η is indeed proportional to $g^{(2)}(0)$ and can be used as a measure for it.

As demonstrated here, η can be easily measured by just observing NIR laser output and SHG intensities, but is a powerful quantity that enables one to access the $g^{(2)}(0)$ of nanolasers without being limited by finite timing resolutions of detectors. The accuracy of the $g^{(2)}(0)$ evaluation using η is currently limited by the instability of the detection setup, and could be improved by using a more stable setup. One disadvantage of this method is the lack of information on the absolute $g^{(2)}(0)$ values, but this can be compensated by a single point calibration using another $g^{(2)}(0)$ measurement. The requirements for nanolasers in order to efficiently induce SHG, such as high Q/V value and large second-order nonlinearity, are often fulfilled by widely investigated high-β nanolasers based on III-V semiconductors. Therefore, the presented method will be useful for characterizing intensity noise properties of various types of nanolasers.

IV. CONCLUSION

In conclusion, we demonstrate a $g^{(2)}(0)$ measurement of a high-β ($=0.12$) nanolaser below and above the lasing threshold using the SHG occurring in the laser cavity. We used the efficiency of SHG, η, which is proved to be proportional to $g^{(2)}(0)$ under conditions where the related experiments are commonly performed. We succeeded in detecting the SHG signals even below the NIR lasing threshold, where only 0.07 photons exist in the NIR cavity mode on average. Then, we compared the experimentally measured η's with $g^{(2)}(0)$ values obtained by the HBT setup and found a good proportionality between them as we initially expected. This demonstrates the validity of the presented method for measuring $g^{(2)}(0)$. It is also worth noting that the measured $g^{(2)}(t)$ curves exhibited oscillations [19,25] as predicted in the recent literature [17].

This work could be extended to the realization of an on-chip quantum intensity correlator [56]. A combination of a Mach-Zehnder interferometer with tunable delay lines [57] and a nonlinear nanocavity exhibiting strong intracavity SHG may enable the measurement of $g^{(2)}(t)$ of light propagating in the integrated optical circuit [31]. Another prospect is the application to higher order intensity correlation measurements, as previously demonstrated for bulky lasers incorporating nonlinear crystals [31]. For the extension to measuring the third-order intensity correlation, one measures the efficiency of third harmonic generation or the intensity correlation between the SHG and the fundamental laser light. In similar ways, one could measure higher order intensity correlations. Application to cavity quantum electrodynamics studies is also a fascinating possibility [58,59]. In particular, our method could be directly applicable to probe multiphoton generation and multiphoton intensity correlation spectra [60–63] in QD-nanocavity coupled systems that have been intensively discussed recently.

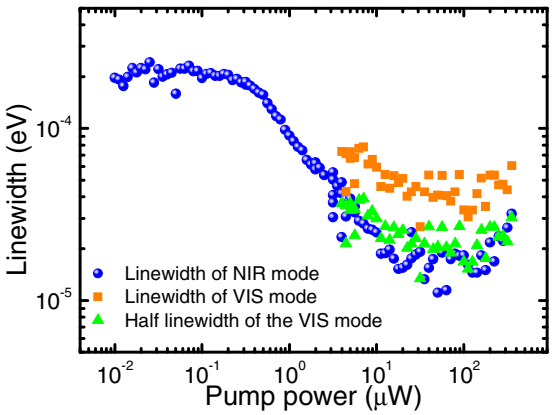

FIG. 6. (Color online) Evolution of the emission linewidth under various pumping powers for the fundamental lasing mode (shown as blue spheres) and second harmonic mode (shown as orange squares). The data is obtained from measurements on another QD nanolaser based on a L3 PhC nanocavity. The green triangular points show half of the VIS emission linewidth, exhibting good agreement with the fundamental mode linewidths.

ACKNOWLEDGMENTS

The authors thank M. Holmes, H. Takagi, S. Kako, and K. Kamide for fruitful discussions. This work was supported by the Project for Developing Innovation Systems and KAKENHI 24760037 of MEXT, Japan, and by JSPS through its FIRST Program.

APPENDIX A: SPECTRAL LINEWIDTH OF THE SHG

We measured the evolution of the emission linewidths of the NIR and VIS modes from another QD nanolaser based on a L3-type PhC nanocavity using high-resolution spectrometers. The nanolaser design and basic characteristics in a similar device are found in our previous report [46]—its basic properties are similar to the nanolaser studied in the main text. Figure 6 shows the measured linewidths of both the fundamental lasing mode and of the SHG light. We observed linewidth narrowing of the NIR mode around the lasing threshold of 10 μW. At the same time, the VIS emission also shows a linewidth narrowing. The green triangular points in Fig. 6 show half of the linewidth of the VIS emission line, exhibiting reasonable agreement with the fundamental mode counterpart. The fact that the VIS linewidth is twice the NIR linewidth can be naturally expected for the SHG light arising from single-mode damped harmonic oscillators. The fundamental mode oscillation $e^{i\omega t-\kappa t}$ is squared to produce the damped nonlinear polarization of $e^{i2\omega t-2\kappa t}$, which is the source of the SHG and decays at twice the rate of the fundamental mode (ω and κ are the oscillation frequency and damping rate, respectively). The doubled linewidth for the SHG spectrum is also well reproduced using master-equation-based calculations using Eq. (3).

APPENDIX B: FITTING TO OSCILLATORY $g^{(2)}(t)$ CURVES

We analyzed the measured $g^{(2)}(t)$ curves by following the procedure presented in Refs. [13,25]. First, solutions of

Eq. (12) are separated into those of the steady state and from the fluctuation by writing $n = n_0 + \delta n$ and $N = N_0 + \delta N$. Substituting these into Eq. (12) and linearizing the resulting equations around the steady state, we obtain the following equations expressing the time evolution of the fluctuations, δn and δN:

$$\begin{aligned} \frac{d\delta n}{dt} &= -\frac{\kappa}{n_0+1}\delta n + \beta\gamma(n_0+1)\delta N, \\ \frac{d\delta N}{dt} &= -\beta\gamma N_0 \delta n - \gamma(1+\beta n_0)\delta N. \end{aligned} \tag{B1}$$

One can easily solve these equations to obtain an expression for $\delta n(t)$ and successively for $g^{(2)}(t)$ [$=1 + \langle \delta n(0)\delta n(t)\rangle / n_0^2$]. A resulting $g^{(2)}(t)$ solution suitable for fitting monotonically decaying curves is $g^{(2)}(t) = 1 + [g^{(2)}(0) - 1]e^{-\gamma_r |t|}$, where γ_r is the damping rate. The oscillating curves are well fitted by another solution, $g^{(2)}(t) = 1 + [g^{(2)}(0) - 1]e^{-\gamma_r |t|}\cos(\omega_r |t| + \phi_0)/\cos(\phi_0)$, where ω_r is the resonance angular frequency of the relaxation oscillation and ϕ_0 is an initial condition. Within this treatment, $g^{(2)}(0)$ is merely an initial condition and cannot be predicted (another sophisticated treatment can predict the value [17]), but ω_r and γ_r may have analytical expressions as follows:

$$\omega_r = \sqrt{\beta\gamma\kappa n_0 - \frac{1}{4}\left(\frac{\kappa}{n_0+1} - \gamma(1+\beta n_0)\right)^2}, \tag{B2}$$

$$\gamma_r = \frac{1}{2}\left(\frac{\kappa}{n_0+1} + \gamma(1+\beta n_0)\right). \tag{B3}$$

We set $g^{(2)}(0)$, ω_r, γ_r, and ϕ_0 as major fitting parameters and fit the experimentally obtained curves using the above two solutions after taking into account the temporal resolution of our HBT setup (~56 ps). The experimental data taken under the pump power below 2 μW were fitted as monotonically decaying curves, while clear relaxation oscillations were observed up to 25 μW. In Fig. 4, some of the fitting results are overlaid to the experimental counterparts. Through the fit, ω_r and γ_r are extracted and plotted in Fig. 7. We found an almost-monotonic increase of $\omega_r/2\pi$ from 1.5 to 6.5 GHz as the pump power increases from 2.4 to 25 μW, and

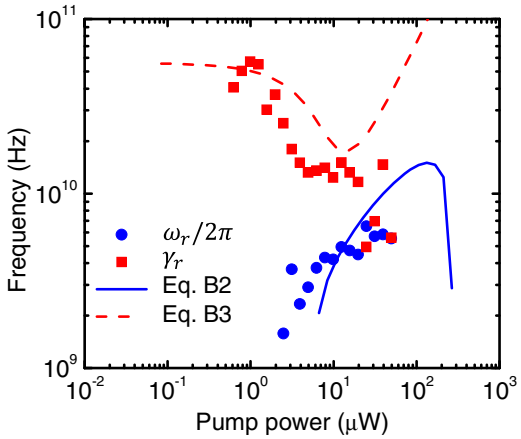

FIG. 7. (Color online) Extracted ω_r and γ_r through the fitting, compared with those calculated using Eqs. (B2) and (B3).

an almost-monotonic decrease of γ_r from 50 to 12 GHz for the pump power from 0.8 to 20 μW. For a comparison, we also calculated ω_r and γ_r, respectively, using Eqs. (B2) and (B3). For this calculation, we used the same constants used for simulating the LL curve in Fig. 3(a) with Eq. (12) ($\kappa = 66$ GHz, $\gamma = 8$ GHz, $\beta = 0.12$) and photon numbers evaluated at the steady state, n_0. $\gamma = 8$ GHz is chosen so that the calculated values and experimental data match well. This relatively fast decay rate may be explained by the Purcell effect in the nanolaser cavity. The calculated results (solid and dashed lines) are plotted in Fig. 7 and show modest agreement with the experimental counterpart (circular and square points), suggesting that the presented modeling of the relaxation oscillation is partially valid for our nanolaser. Remaining deviations in the plot indicate the necessity of further experimental and theoretical work in order to fully understand the relaxation oscillation in high-β nanolasers: The topic is closely related to some important issues such as the intensity modulation bandwidth of high-β nanolasers under small signal modulation [3]. However, such pursuit is out of the scope of this paper.

[1] O. Painter, R. Lee, A. Scherer, A. Yariv, J. O'Brien, P. Dapkus, and I. Kim, Science **284**, 1819 (1999).

[2] M. Loncar, T. Yoshie, A. Scherer, P. Gogna, and Y. Qiu, Appl. Phys. Lett. **81**, 2680 (2002).

[3] H. Altug, D. Englund, and J. Vuckovic, Nat. Phys. **2**, 484 (2006).

[4] S. M. Ulrich, C. Gies, S. Ates, J. Wiersig, S. Reitzenstein, C. Hofmann, A. Löffler, A. Forchel, F. Jahnke, and P. Michler, Phys. Rev. Lett. **98**, 043906 (2007).

[5] M. Nomura, S. Iwamoto, K. Watanabe, N. Kumagai, Y. Nakata, S. Ishida, and Y. Arakawa, Opt. Express **14**, 6308 (2006).

[6] K. Nozaki, S. Kita, and T. Baba, Opt. Express **15**, 7506 (2007).

[7] M. T. Hill, Y.-S. Oei, B. Smalbrugge, Y. Zhu, T. de Vries, P. J. van Veldhoven, F. W. M. van Otten, T. J. Eijkemans, J. P. Turkiewicz, H. de Waardt, E. J. Geluk, S.-H. Kwon, Y.-H. Lee, R. Nötzel, and M. K. Smit, Nat. Photonics **1**, 589 (2007).

[8] M. P. Nezhad, A. Simic, O. Bondarenko, B. Slutsky, A. Mizrahi, L. Feng, V. Lomakin, and Y. Fainman, Nat. Photonics **4**, 395 (2010).

[9] R. F. Oulton, V. J. Sorger, T. Zentgraf, R.-M. Ma, C. Gladden, L. Dai, G. Bartal, and X. Zhang, Nature(London) **461**, 629 (2009).

[10] Y.-J. Lu, J. Kim, H.-Y. Chen, C. Wu, N. Dabidian, C. E. Sanders, C.-Y. Wang, M.-Y. Lu, B.-H. Li, X. Qiu, W.-H. Chang, L.-J. Chen, G. Shvets, C.-K. Shih, and S. Gwo, Science **337**, 450 (2012).

[11] G. Bjork and Y. Yamamoto, IEEE J. Quantum Electron. **27**, 2386 (1991).

[12] P. R. Rice and H. J. Carmichael, Phys. Rev. A **50**, 4318 (1994).
[13] N. J. van Druten, Y. Lien, C. Serrat, S. S. R. Oemrawsingh, M. P. van Exter, and J. P. Woerdman, Phys. Rev. A **62**, 053808 (2000).
[14] D. Elvira, X. Hachair, V. B. Verma, R. Braive, G. Beaudoin, I. Robert-Philip, I. Sagnes, B. Baek, S. W. Nam, E. A. Dauler, I. Abram, M. J. Stevens, and A. Beveratos, Phys. Rev. A **84**, 061802 (2011).
[15] S. Ates, C. Gies, S. M. Ulrich, J. Wiersig, S. Reitzenstein, A. Loffler, A. Forchel, F. Jahnke, and P. Michler, Phys. Rev. B **78**, 155319 (2008).
[16] C. Gies, J. Wiersig, M. Lorke, and F. Jahnke, Phys. Rev. A **75**, 013803 (2007).
[17] A. Lebreton, I. Abram, N. Takemura, M. Kuwata-Gonokami, I. Robert-Philip, and A. Beveratos, New J. Phys. **15**, 033039 (2013).
[18] Y.-S. Choi, M. T. Rakher, K. Hennessy, S. Strauf, A. Badolato, P. M. Petroff, D. Bouwmeester, and E. L. Hu, Appl. Phys. Lett. **91**, 031108 (2007).
[19] J. Wiersig, C. Gies, F. Jahnke, M. Assmann, T. Berstermann, M. Bayer, C. Kistner, S. Reitzenstein, C. Schneider, S. Höfling, A. Forchel, C. Kruse, J. Kalden, and D. Hommel, Nature (London) **460**, 245 (2009).
[20] J.-S. Tempel, I. A. Akimov, M. Assmann, C. Schneider, S. Höfling, C. Kistner, S. Reitzenstein, L. Worschech, A. Forchel, and M. Bayer, J. Opt. Soc. Am. B **28**, 1404 (2011).
[21] A. Lebreton, I. Abram, R. Braive, I. Sagnes, I. Robert-Philip, and A. Beveratos, Phys. Rev. Lett. **110**, 163603 (2013).
[22] M. J. Stevens, B. Baek, E. A. Dauler, A. J. Kerman, R. J. Molnar, S. A. Hamilton, K. K. Berggren, R. P. Mirin, and S. W. Nam, Opt. Express **18**, 1430 (2010).
[23] M. Ueda, M. Kuwata, N. Nagasawa, T. Urakami, Y. Takiguchi, and Y. Tsuchiya, Opt. Commun. **65**, 315 (1988).
[24] M. Assmann, F. Veit, M. Bayer, M. van der Poel, and J. M. Hvam, Science **325**, 297 (2009).
[25] N. Takemura, J. Omachi, and M. Kuwata-Gonokami, Phys. Rev. A **85**, 053811 (2012).
[26] G. Roumpos and S. T. Cundiff, Opt. Lett. **38**, 139 (2013).
[27] G. Roumpos and S. T. Cundiff, J. Opt. Soc. Am. B **30**, 1303 (2013).
[28] F. Boitier, A. Godard, E. Rosencher, and C. Fabre, Nat. Phys. **5**, 267 (2009).
[29] Y. Qu and S. Singh, Opt. Commun. **90**, 111 (1992).
[30] Y. Qu and S. Singh, Phys. Rev. A **51**, 2530 (1995).
[31] Y. Qu, S. Singh, and C. D. Cantrell, Phys. Rev. Lett. **76**, 1236 (1996).
[32] T. J. Kippenberg, S. M. Spillane, and K. J. Vahala, Phys. Rev. Lett. **93**, 083904 (2004).
[33] T. Carmon and K. J. Vahala, Nat. Phys. **3**, 430 (2007).
[34] P. S. Kuo, J. Bravo-Abad, and G. S. Solomon, Nat. Commun. **5**, 3109 (2014).
[35] M. Foster, A. Turner, M. Lipson, and A. L. Gaeta, Opt. Express **16**, 1300 (2008).
[36] D. Duchesne, K. A. Rutkowska, M. Volatier, F. Légaré, S. Delprat, M. Chaker, D. Modotto, A. Locatelli, C. De Angelis, M. Sorel, D. N. Christodoulides, G. Salamo, R. Arès, V. Aimez, and R. Morandotti, Opt. Express **19**, 12408 (2011).
[37] S. Kim, J. Jin, Y.-J. Kim, I.-Y. Park, Y. Kim, and S.-W. Kim, Nature (London) **453**, 757 (2008).
[38] P. Genevet, J.-P. Tetienne, E. Gatzogiannis, R. Blanchard, M. A. Kats, M. O. Scully, and F. Capasso, Nano Lett. **10**, 4880 (2010).
[39] M. W. McCutcheon, J. F. Young, G. W. Rieger, D. Dalacu, S. Frédérick, P. J. Poole, and R. L. Williams, Phys. Rev. B **76**, 245104 (2007).
[40] K. Rivoire, Z. Lin, F. Hatami, W. T. Masselink, and J. Vuckovic, Opt. Express **17**, 22609 (2009).
[41] B. Corcoran, C. Monat, C. Grillet, D. J. Moss, B. J. Eggleton, T. P. White, L. O'Faolain, and T. F. Krauss, Nat. Photonics **3**, 206 (2009).
[42] K. Rivoire, Z. Lin, F. Hatami, and J. Vuckovic, Appl. Phys. Lett. **97**, 043103 (2010).
[43] M. Galli, D. Gerace, K. Welna, T. F. Krauss, L. O'Faolain, G. Guizzetti, and L. C. Andreani, Opt. Express **18**, 26613 (2010).
[44] K. Rivoire, S. Buckley, F. Hatami, and J. Vuckovic, Appl. Phys. Lett. **98**, 263113 (2011).
[45] S. Buckley, M. Radulaski, K. Biermann, and J. Vuckovic, Appl. Phys. Lett. **103**, 211117 (2013).
[46] Y. Ota, K. Watanabe, S. Iwamoto, and Y. Arakawa, Opt. Express **21**, 19778 (2013).
[47] Y. Ota, K. Watanabe, S. Iwamoto, and Y. Arakawa, Appl. Phys. Lett. **103**, 243115 (2013).
[48] Y. Shen, Phys. Rev. **155**, 921 (1967).
[49] P. Mandel and X.-G. Wu, J. Opt. Soc. Am. B **3**, 940 (1986).
[50] M. J. Collett and R. B. Levien, Phys. Rev. A **43**, 5068 (1991).
[51] R. B. Levien, M. J. Collett, and D. F. Walls, Phys. Rev. A **47**, 2324 (1993).
[52] Z. Ou and H. Kimble, Opt. Lett. **18**, 1053 (1993).
[53] P. Yao, P. K. Pathak, E. Illes, S. Hughes, S. Münch, S. Reitzenstein, P. Franeck, A. Löffler, T. Heindel, S. Höfling, L. Worschech, and A. Forchel, Phys. Rev. B **81**, 033309 (2010).
[54] M. Nomura, K. Tanabe, S. Iwamoto, and Y. Arakawa, Opt. Express **18**, 8144 (2010).
[55] G. Bjork, A. Karlsson, and Y. Yamamoto, Phys. Rev. A **50**, 1675 (1994).
[56] R. W. Heeres, L. P. Kouwenhoven, and V. Zwiller, Nat. Nanotechnol. **8**, 719 (2013).
[57] N. Ishikura, T. Baba, E. Kuramochi, and M. Notomi, Opt. Express **19**, 24102 (2011).
[58] M. W. McCutcheon, D. E. Chang, Y. Zhang, M. D. Lukin, and M. Loncar, Opt. Express **17**, 22689 (2009).
[59] A. Majumdar and D. Gerace, Phys. Rev. B **87**, 235319 (2013).
[60] Y. Ota, S. Iwamoto, N. Kumagai, and Y. Arakawa, Phys. Rev. Lett. **107**, 233602 (2011).
[61] A. Reinhard, T. Volz, M. Winger, A. Badolato, K. J. Hennessy, E. L. Hu, and A. Imamoglu, Nat. Photonics **6**, 93 (2011).
[62] A. Majumdar, M. Bajcsy, and J. Vučković, Phys. Rev. A **85**, 041801 (2012).
[63] E. del Valle, A. Gonzalez-Tudela, F. P. Laussy, C. Tejedor, and M. J. Hartmann, Phys. Rev. Lett. **109**, 183601 (2012).